Acta Technica *62* (2017), No. 7A, 1719–1732

A Network Coding Algorithm for Sense Awareness of Internet of Things

Youwei Shao[1]

Abstract. In order to improve the quality of video transmission in heterogeneous network and take full account of the loss of data transmission caused by channel instability, a joint source-channel coding method of heterogeneous network video based on the lattice quantization is proposed. Firstly, a multiple-description independent parallel channel transmission framework for Gaussian video source transmission is established by using the signal-source parallel channel transmission scheme of multiple description joint source-channel coding. Secondly, the lattice-scale quantization method is used to reduce the simulation mapping bandwidth with or without SI decoder to improve performance of heterogeneous network video transmission through the bandwidth extension. Finally, the effectiveness of the proposed method is verified by comparative test in the code redundancy, code rate, peak signal to noise ratio, end-to-end video frame delay and effective loss rate indicator.

Key words. Scale quantization, Heterogeneous networks, Joint source, Channel coding, Energy consumption.

1. Introduction

In recent years, video transmission (such as live broadcasting of online game, video conference, live sports, etc.) based on mobile technologies has become a popular streaming media application, and video transmission traffic also shows rapid growth [1]. Video traffic in 2012 accounted for about 58% of the total traffic, and it will reach about 70% in 2017. From 2012 to 2017, total mobile traffic will be about 14 times. At the end of 2015, the total traffic of super-definition video transmission has exceeded that of the high-definition video transmission [2]. Therefore, how to ensure the reliability of the super-definition video data transmission under the existing network is a major challenge for service providers.lthough the current network infrastructure construction has provided users with different Internet access methods (such as WiMAX, W LAN and cellular networks), the data transmission

[1]School of Architecture and Materials, Chongqing College of Electronic Engineering, Chongqing, China

capability of the network in a single form is still limited and cannot provide satisfactory mobile video transmission performance [3]. The main problems in WLAN networks are limited bandwidth and small coverage, so it cannot meet the demands of a large number of mobile users in mobile video services. WiMAX network can provide relatively wider coverage and higher peak rate, but it cannot meet the demand for real-time high-throughput multimedia when the user share is large. The limited performance of a single network makes the integration of heterogeneous network bandwidth get more attention of scholars, and there have been many research results. The main research topics of the classic joint source-channel coding [4] (JSCC) are the rate optimization of channel coding and source, the error correction coding of video data and the channel state. Specific work includes: (1) optimization of the ratio of coding channel to source coding, as described in the literature [5-6]; (2) how to adjust the code rate to realize the desired transmission target in case that the channel parameters and state, as described in the literature [7]; (3) reliability improvement of channel coding, such as fountain code, Turbo, LDPC, Reed-Solomon, etc. [8-10]. (4) Joint coding optimization algorithm design is combined with transmission control, error concealment, error control and other methods to improve the system performance, as described in the literature [11]; literature [12] studies the optimization of the coding rate under bandwidth limitation and the video end-to-end distortion can be minimized. Literature [13] studies the JSCC scheme of video transmission in layered heterogeneous devices to maximize the mean value of video transmission quality.

However, the above algorithm utilizes the error control method, without considering the fault of the channel itself, which easily results in the weakening of the video transmission quality of the transmitted data and affect the user experience and the video service quality. In this regard, this paper focuses on heterogeneous network video transmission to study the multiple description joint source-channel coding method with the aid of the lattice quantization conversion in the decoder to obtain low distortion and low delay video transmission scheme.

2. Problem model description

Fig.1 shows the parallel channel transmission scheme of signal-source heterogeneous network based on the multiple description joint source-channel coding (MD-JSCC).

In the figure, each data block $s^n \in \mathcal{R}^n$ of n source symbol is coded into two codewords $x_1^{\beta_1 n}(s^n) \in \chi_1^{n\beta_1}$, $x_1^{\beta_2 n}(s^n) \in \chi_1^{n\beta_2}$ in which β_i refers to bandwidth ratio, such as ratio of channel symbol to source symbol, χ_i represents some limited alphabet sets are transmitted through two independent noisy channels. The decoder 1, 2, 0 receive $y_1^{\beta_l n}, y_2^{\beta_2 n}$ and $\left(y_1^{\beta_l n}, y_2^{\beta_2 n}\right)$ and use distortion $D_i, i = 0, 1, 2$ to reconstruct s^n, namely:

$$d_i(s^n, \hat{s}_i^n) = \frac{1}{n}\sum_{k=1}^{n} d_i(s_k, \hat{s}_k) \le D_i \,. \tag{1}$$

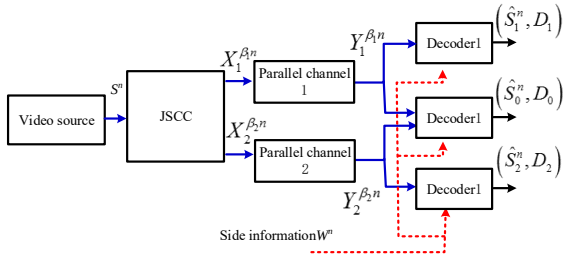

Fig. 1. MD-JSCC parallel transmission scheme

Where, d_i: $R \times R \to [0, \infty)$ are some distortion measures. (D_1, D_2) and D_0 are respectively called side distortion and center distortion. When side information W^n is available in the decoder, these additional information can be combined with the side information to reduce the corresponding distortion.

If there is no noise in the channel, the above problem is degraded to a Multiple Description Source Coding (MD-SC) issue. In this case, $\left(2^{nR_1}, 2^{nR_2}, n\right)$ the coding consists of the following:

(1) Two encoders, of which encoder 1 assigns an index $m_1(s^n) \in [1 : 2^{nR_1})$ to each source sequence and encoder 2 assigns an index $m_2(s^n) \in [1 : 2^{nR_2})$ to each source sequence;

(2) Three decoders, where the decoder $i = 1, 2$ observes and receives the index m_i and side information ω^n and evaluates $\hat{s}_i^n$. Decoder 0 evaluates $\hat{s}_0^n$ after receiving index pair (m_1, m_2) and side information ω^n.

If there is a $\left(2^{nR_1}, 2^{nR_2}, n\right)$ sequence encoding which satisfies the following conditions:

$$\limsup_{n\to\infty} E\left(d_i\left(s^n, \hat{s}_i^n\right)\right) \le D_i, i = 0, 1, 2\,. \tag{2}$$

The rate-distortion quintuple $(R_1,\ R_2,\ D_0,\ D_1,\ D_2)$ will be achievable. The rate-distortion region$\mathcal{R}(D_0, D_1, D_2)$ of the MD-SC problem is a closure set of rate to (R_1, R_2). The presence or absence of side information (SI) in this region is unknown in advance. The exception is the quadratic Gauss MD-SC case, the Gaussian source and quadratic distortion function:

$$d\left(s^n, \hat{s}^n\right) = \frac{1}{n}\sum_{k=1}^{n}\left(s_k - \hat{s}_k\right)^2. \tag{3}$$

Consider traversing parallel channels (e.g. AWGN channels) and SI-free decoder, as shown in Fig.1. Under this assumption, a set of achievable distortion sets Γ can be given using a closed set:

$$\begin{aligned}\Gamma = (D_0, D_1, D_2) \in \mathcal{R}_+^3 :\\ \mathcal{R}(D_0, D_1, D_2) \cap \mathcal{R}(C_1, C_2) \ne \emptyset\,.\end{aligned} \tag{4}$$

In the formula (4), $R(C_1, C_2) = \{(R_1, R_2) : R_1 \le C_1, R_2 \le C_2\}$.

3. Simulation MD-JSCC scheme based on lattice quantizer

Consider the communication scheme shown in Fig.1, where the n Gaussian random symbol sequence with zero mean and variance σ_S^2 is $S_k \sim \mathcal{N}\left(0, \sigma_S^2\right)$, $k = 1, 2, \cdots, n$, and they must be transmitted through two parallel noisy channels. Assume that SI information $\{W_k\}$ is independent and identically distributed Gaussian random variable sequence:

$$W_k = S_k + U_k \,. \tag{5}$$

Where, $S_k \sim \mathcal{N}(0, \sigma_S^2)$ and $U_k \sim \mathcal{N}(0, \sigma_U^2)$. The correlation coefficient of S_k and W_k can be calculated as $\rho_{S,W} = \sigma_S \Big/ \sqrt{\sigma_S^2 + \sigma_U^2}$.

The joint source-channel MD encoder maps the input sequence to two-channel codewords $\boldsymbol{X}_i = [X_{i,1}, \cdots, X_{i,\beta_i n}]$, $i = 1, 2$.

$$\begin{cases} g_1 : \mathcal{S}^n \to \chi_1^{\beta_1 n} \\ g_2 : \mathcal{S}^n \to \chi_2^{\beta_2 n} \end{cases} \tag{6}$$

3.1. Simulation mapping of multiple description

As the total bandwidth ratio required for a proposed JSCC is $\beta = \beta_1 + \beta_2 \geq 1$, the liner mapping can be regarded as a sub-mapping block that can be used continuously with lattice scaling. Fig.2 shows the algorithm structure of the mapping process, where (S_k, S_{k+1}) represents the source sample.

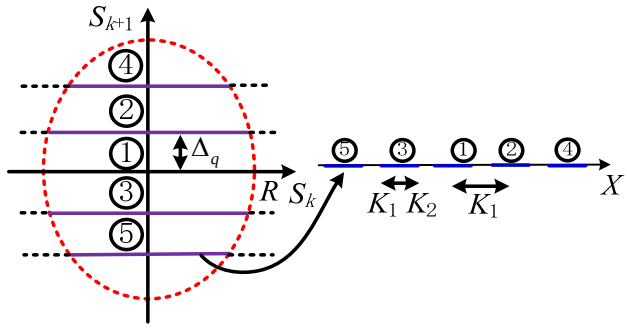

Fig. 2. Bandwidth reduction simulation mapping

The method uses scalar quantization to encode the sample S_{k+1}, and $X_k \in \mathcal{R}$ can be obtained after the quantized sample is overlaid and mapped with other samples. By considering uniform (scalar) quantization and horizontal step quantization, we get $i_{S_{k+1}} \in 0, \pm 1, \cdots, \pm N_q$ as S_{k+1} quantitative indicator:

$$i_{S_{k+1}} = round\left[\frac{S_{k+1}}{\Delta_q}\right] . \tag{7}$$

Indicator $i_{S_{k+1}}$ and sample S_k can be mapped as channel symbols X_k as below:

$$\begin{aligned} X_k &= G\left(S_k, S_{k+1}\right) \\ &\cong K_1\left(i_{S_{k+1}} + K_2\left(-1\right)^{i_{S_{k+1}}} \cdot l_{i_{S_{k+1}}}\left(S_k\right)\right) \end{aligned} \tag{8}$$

Where K_1 is a normalized constant that can be created as a power constraint $E(X^2) \leq P$, $K_2 \in [0,1)$ specifies the interval width in the signal space and can be expressed as S_k. In order to make the signal space mapping effective, the hard-clipping function $l_{i_{s_{k+1}}}(\cdot)$ is used to limit the dynamic range S_k of the signal, which can be expressed as below:

$$l_{i_{s_{k+1}}}(S_k) = \frac{sgn(S_k)}{2} \cdot \min\left(1, \frac{|S_k|}{\sqrt{R^2 - (\Delta_q \cdot i_{s_{k+1}})^2}}\right). \tag{9}$$

Where the parameter R gives the maximum dynamic range of the sample (S_k, S_{k+1}). The number N_q of quantization levels is set as $N_q = R/\Delta_q$.

3.2. Lattice quantizer

l-dimensional lattice is a discrete subgroup of Euclidean space and can be described as below:

$$\Lambda \cong \left\{\lambda = \Psi \cdot b : \ b \in Z^l\right\}. \tag{10}$$

In the formula, the rank of generator matrix $\Psi \in R^{l \times l}$ is l.

Definition 1: (lattice quantizer) $Q_\Lambda : R^l \to \Lambda$ that maps a point R^l to the closest point from the Euclidean distance in Λ:

$$Q_\Lambda(y) \cong \arg\min_{\lambda \in \Lambda} \|y - \lambda\|. \tag{11}$$

In addition, the modular arithmetic form of $y \in R^l$ to Λ is defined as below:

$$\boldsymbol{y} \mathrm{mod} \Lambda = \boldsymbol{y} - Q_\Lambda(\boldsymbol{y}). \tag{12}$$

Definition 2: (basic Voronoi region) This region can be expressed as $\mathcal{V}_\Lambda$ and it is the point set in R^l:

$$\mathcal{V}_\Lambda = \left(\boldsymbol{y} : \boldsymbol{y} \in R^l, Q_\Lambda(\boldsymbol{y}) = 0\right\}. \tag{13}$$

Define the volume $Vol\left(\Lambda\right)$ of the lattice Λ, which is calculated as $Vol\left(\Lambda\right) = \det\left(\Psi\right)$. The proposed coding scheme is based on a continuous scale lattice, $\{\delta_j \Lambda\}_{j=1}^{m-1}$ where $\delta_1 > \delta_2 > \cdots > \delta_{m-1}$, $\delta_j \in R_+$ is the scale factor used in every m steps.

Definition 3: (Scale) assuming that Λ is l-dimensional lattice and $\delta \in R$ is the scalar of real part, then $\delta\Lambda \cong \{\delta\lambda : \lambda \in \Lambda\}$ is also a lattice.

Since the dimension of the input vector of simulated and mapped in Fig.2 is $l = 2$, it is only necessary to limit the lattice to a two-dimensional form. Therefore, Λ is

selected as the lattice:

$$\Psi = \begin{bmatrix} 1 & 1/2 \\ 0 & \sqrt{3}/2 \end{bmatrix} . \tag{14}$$

3.3. Coding - decoding process

As the source sequences are independently and identically distributed, consider the first pair (S_1, S_2) of source symbols encoded by complementary simulation encoding functions (joint source-channel coding) $g_i : R \times R \to R^m \, (i = 1, 2)$ to produce the channel symbols:

$$\boldsymbol{X}_i = (X_{i,1}, X_{i,2}, \cdots, X_{i,m}) = g_i(S_1, S_2) . \tag{15}$$

As $\beta_1 = \beta_2 = m/2$, the total bandwidth ratio is $\beta = m$. g_1 is similar to g_2 in the construction, however, the rotation R of the input source symbol (S_1, S_2) is applied to g_2 for description as independent as possible:

$$g_2(S_1, S_2) = g_1 \left(\boldsymbol{R} \cdot (S_1, S_2) \right) . \tag{16}$$

$$\boldsymbol{R} = \begin{bmatrix} \cos\theta & -\sin\theta \\ \sin\theta & \cos\theta \end{bmatrix} . \tag{17}$$

Where, θ is the rotation angle. The maximum correlation output can be obtained using the rotation angle $\theta = \pi/2$, as shown in literature [15]. The proposed joint simulation source channel MD coding scheme is shown in Fig.3.

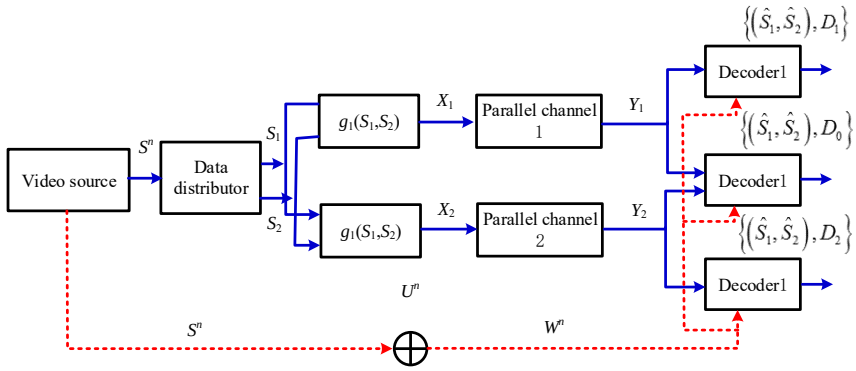

Fig. 3. Joint simulation source channel MD coding scheme

In Fig.3, (S_1, S_2) can encode $\boldsymbol{X}_1$ according to the following steps:

Case 1: (without available SI encoder) For simplicity, assume that the optimal scale factor $\{\delta_j\}_{j=1}^{m-1}$ has been worked out (as described in Section 3.4). Define the initial pair $(Z_1, Z_2)_0 \cong (S_1, S_2)$ of auxiliary variables. The first code symbol can be calculated as: $X_{1,1} = G(L_0 \cdot (Z_1, Z_2)_0)$, where, $G(\cdot)$ is shown in formula (8) and $L_0 = 0$. For $j \in (1, 2, \cdots, m-1)$, the iterative calculation process is as follows:

(1) Calculate $(Z_1, Z_2)_j$:

$$(Z_1, Z_2)_j \cong (Z_1, Z_2)_{j-1} \bmod \delta_j \Lambda \,. \tag{18}$$

The above formula shows that $(Z_1, Z_2)_j$ depends on the basic Voronoi region $V_{\delta\Lambda}^{(j)}$ of the lattice $\delta_j \Lambda$.

(2) Set the channel symbol symbol. As shown in Fig.4, we can get the following by considering the radius of the linear mapping circle and normalizing $(Z_l, Z_2)_j$ with the scale factor L_j:

$$L_j = \sqrt{\frac{\pi R^2}{Vol(\delta_j \Lambda)}} \,. \tag{19}$$

At the end of the encoding process, we can get the following:

$$g_1(S_1, S_2) = (G(L_0 \cdot (Z_1, Z_2)_0), \cdots, G(L_{m-1} \cdot (Z_1, Z_2)_{m-1})) \,. \tag{20}$$

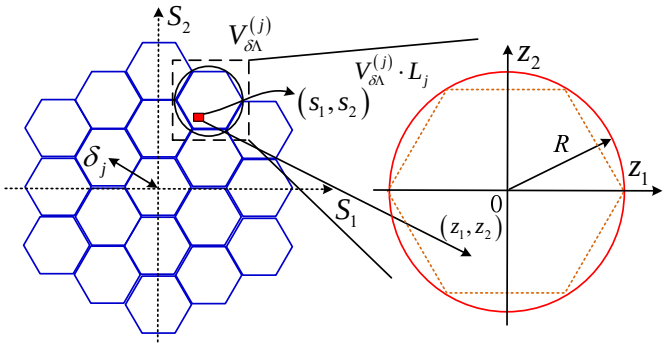

Fig. 4. Hexagonal lattice transformation process

Case 2: (with available SI encoder) The encoding algorithm will follow the process in case 1, except for the initial pair $(Z_1, Z_2)_0$ of ancillary variables whose alternative calculation is as below:

$$(Z_1, Z_2)_0 = (S_1, S_2) \bmod \delta_0^{(si)} \Lambda \,. \tag{21}$$

The first channel symbol can be calculated as: $X_{l,1} = G(L_0^{(si)} \cdot (Z_1, Z_2)_0)$. The remaining channel symbols $X_{1,2}, X_{1,3}, \cdots, X_{1,m}$ can be obtained according to the calculation process in case 1.

Case 3: (without available SI decoder) The three decoders perform a Minimum Mean Squared Error (MMSE) on the estimator based on the received symbol $_1$ and $\boldsymbol{Y}_2$. The estimation process is shown in Fig. 5.

(1) Symbol decoding: for $j \in (0, 1, \cdots, m-1)$, the side decoder $i = 1, 2$ calculates the MMSE estimate $(\hat{Z}_1, \hat{Z}_2)_j^{(i)} = E\left[(Z_1, Z_2)_j | Y_{i,1+j}\right]$. Center decoder $i = 0$ calculates $(\hat{Z}_1, \hat{Z}_2)_j^{(0)} = E\left[(Z_1, Z_2)_j | Y_{1,1+j}, Y_{2,1+j}\right]$. After the calculation is completed, the estimate of the source symbols (S_1, S_2) for each decoder $i = 0, 1, 2$ can

be calculated according to Fig. 5:

$$(\hat{S}_1, \hat{S}_2)^i = \\ = \sum_{l=0}^{m-2} Q_{\delta_{l+1}\Lambda}((\hat{Z}_1, \hat{Z}_2)_l^{(i)}) + (\hat{Z}_1, \hat{Z}_2)_{m-1}^{(i)}. \tag{22}$$

(2) Joint decoder: The source symbol (S_1, S_2) is estimated as: for the side decoder $i = 1, 2$, there is $(\hat{S}_l, \hat{S}_2)^i = E[(S_1, S_2)|Y_i]$, and $(\hat{S}_1, \hat{S}_2)^0 = E[(S_1, S_2)|Y_1, Y_2]$ for the center decoder $i = 0$.

Case 4: (with available SI decoder) For simplicity, only the joint decoding of the optimal estimate are considered herein, so MMSE can be used for (S_1, S_2) estimation, that is, there is $(\hat{S}_l, \hat{S}_2)^i = E[(S_1, S_2)|Y_i, W_1, W_2]$ for the side decoder, and $(\hat{S}_1, \hat{S}_2)^0 = E[(S_1, S_2)|Y_1, Y_2, W_1, W_2]$ for the center decoder $i = 0$. Since $Y_i \leftrightarrow (S_1, S_2) \leftrightarrow (W_1, W_2)$ forms a Markov chain, it is easy to calculate the aforementioned expectation.

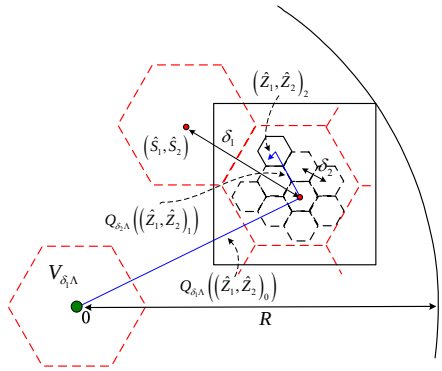

Fig. 5. Graphical interpretation of symbolic decoder (m = 3)

3.4. Offline calculation of scale factor

For the prescribed $m = M$, $\{\delta_j\}_{j=1}^{M-1}$ can be obtained by offline recursion in the following way. The initial value of δ_1 can be obtained by setting $m = 2$ in the above encoding and decoding processes, and then δ_1 is selected (see formula (8)) to minimize the required distortion set. Assuming that $\delta_1, \delta_2, \cdots, \delta_k (k < m - 1)$ have been obtained, then δ_{k+1} can be obtained by setting $m = k + 2$ and using the first $k + 1$ steps of the encoding algorithm. Then in step $k + 2$, choose δ_{k+1} in formula (8) to minimized the expected distortion.

In the case of available SI, the scale factor $\left\{\delta_j^{(si)}\right\}_{j=0}^{m-1}$ can be calculated by setting $m = 1$. When the correlation coefficient $\rho_{S,W}$ between S and W tends to 0, $\delta_0^{(si)} \to \infty$, $\delta_j^{(si)} \to \delta_{j+1}$, then the above scheme degenerates into a case without available SI. On the contrary, the larger $\rho_{S,W}$, the smaller $\delta_j^{(si)}$. Therefore, a

larger correlation means a smaller Voronoi region, indicating that the total distortion decreases as the calculation step j increases.

4. Experimental analysis

4.1. Experimental setting

In the experimental simulation stage of this section, Exata is selected as the network simulator. The simulator is set as follows: The simulation platform version is Exata 2.1, an advanced simulation version developed by QualNet, which can be used for experimental simulation in a semi-physical environment. In order to achieve the purpose of H.264 real-time video streaming, we use Exata2.1 to integrate with the algorithm proposed in this paper for development. For details of development, please refer to the Exata manual. In the network structure design, the wired network access port is reserved, and the wireless network interfaces equipped on the end include WiMAX interface, WLAN interface and HSDPA interface. The connection between client and server can be established by binding IP address. The relevant parameters of the heterogeneous network are listed in Tab.1.

Table 1. Wireless network parameters configuration

Parameter	value	Parameter	value
HSDPA parameter		Subcarrier number	255
SIR target value	10dB	Sampling factor	8/7
orthogonal factor	0.5	SNR mean	16dB
Channel power	33dB	Symbol duration	2048
Maximum station of base station	44dB	Mean loss rate	2.5%
Unit bandwidth	3.85Mc/s	Mean pulse length	15ms
SNIR	0.58	WLAN parameter	
Background noise power	-103dB	Mean bit rate	2Mbps
Mean loss rate	2%	Time slot	10μs
Mean pulse length	10ms	The biggest competition window	32
WiMAX parameter		Mean loss rate	3.5%
System bandwidth	7MHz	Mean pulse length	20ms

4.2. Comparison algorithm selection

This paper compares the proposed SCLQ-JSCC algorithm with the following multipath / heterogeneous network video transmission schemes: (1) Virtual Path System (VPS). This method uses fountain code to construct the heterogeneous network video transmission path. In the algorithm implementation, the parameter is updated every 0.5s. The fountain code has a packet size of 8 Byte and a symbol length of 512 Byte; (2) Media Flow Rate Allocation (MFRA). This strategy uses the maximum utilization rate algorithm to optimize the code rate and redundancy for

multipath video transmission, in which the number of video layers is set as 1 owning to the scalability of SVC / H.264 encoding.

4.3. Result analysis

In order to verify the performance of the proposed SCLQ-JSCC algorithm, the redundancy and the video code rate of forward error correction (FEC) for tolerable transmission loss rate in the indicator selection are compared, as shown in Fig. 6.

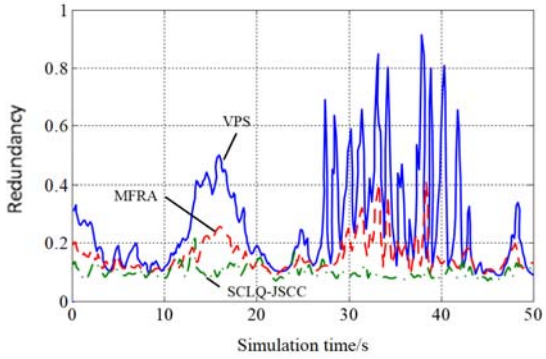

(a) Code redundancy

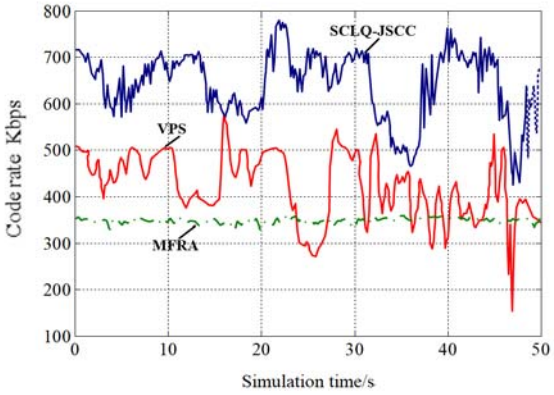

(b) Video code rate

Fig. 6. Algorithm performance analysis

The results of Fig. 6 show the comparison of the three contrast algorithms in terms of redundancy and video code rate. According to Fig.6a, we can see that the proposed SCLQ-JSCC algorithm is significantly superior to VPS and MFRA in terms of code redundancy, and at the same time, MFRA strategy is better than VPS strategy with respect to redundancy since the redundancy optimization is taken into account. As shown in Fig. 6b, we can see that the algorithm in this paper is better than the two contrast strategies selected in the video code rate, while the VPS strategy has higher code rate than the MFRA algorithm because it considers

the virtual path transmission.

The comparison results of standard deviation, mean value and the instantaneous value of the PSNR index (peak signal-to-noise ratio) received in the video during the experiment are shown in Tab.2.

Table 2. Comparison of PSNR indicators received in video

Research object	Indicator classification	VPS	MFRA	SCLQ-JSCC
City	Mean value	36.1	25.3	40.3
	Standard deviation	0.67	0.73	0.56
Crew	Mean value	32.6	25.8	35.3
	Standard deviation	0.75	0.77	0.56
Harbor	Mean value	33.5	25.6	36.1
	Standard deviation	0.71	0.65	0.53
Soccer	Mean value	37.1	30.2	41.5
	Standard deviation	0.96	0.98	0.82

Experimental results in Tab. 2 show that the proposed algorithm in this paper is always superior to VPS and MFRA in the four groups of video transmission such as City in terms of mean PSNR indicator, which indicates that the distortion mixed in the transmission signal is relatively minimum and that video restoration quality of the proposed algorithm is better. Moreover, the standard deviation of PSNR indicator obtained by the proposed algorithm is the smallest, indicating that the proposed algorithm has better stability of video transmission.

Experimental results in Fig. 7 show the cumulative distribution of frame delays during video transmission. According to the experimental results in Fig. 7, the frame delay of the SCLQ-JSCC algorithm proposed in this paper is significantly lower than those of the VPS and MFRA algorithms, which indicates the low latency of the proposed algorithm. Although the VPS algorithm considers the virtual path transmission, the virtual path needs to be re-established after video frame is lost, thereby affecting the transmission delay of the video frame.

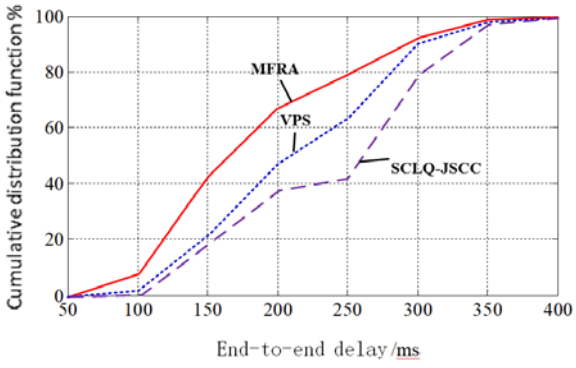

Fig. 7. Cumulative distribution of transmission delay

Fig.8 shows the comparison of the effective loss rate indicators in [30, 80] time

quantum. It should be noted that the PSNR value in the video transmission process is not only related to the loss rate, but also related to the loss of the video frame. Therefore, this indicator can reflect the quality change of the video transmission process to some extent.

As shown in Fig.8, it can be seen that the effective loss rate of proposed algorithm is smaller than those of the selected VPS and MFRA algorithms, and MFRA results in higher loss rate than VPS and SCLQ -JSCC algorithm proposed in this paper due to the video split-stream transmission technology used in MFRA. The above experimental results verify the advantages of the proposed algorithm in video data transmission quality and transmission speed.

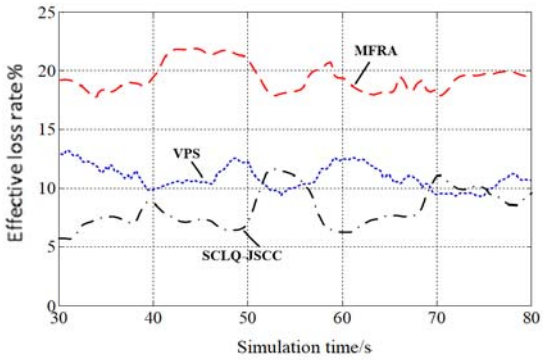

Fig. 8. Effective loss rate indicator

5. Conclusion

In this paper, a joint source-channel coding method of heterogeneous network video based on the lattice quantization is proposed, and a multiple-description independent parallel channel transmission framework for Gaussian video source transmission is established. The simulation mapping bandwidth is reduced with the lattice-scale quantization method, and the performance of heterogeneous network video transmission is improved through the bandwidth extension. Future research direction is mainly the MD-JSCC scheme simulation network topology of the multi-access relay channel or multi-hop network.

Acknowledgement

Science and technology research project of the Chongqing Municipal Education Committee (KJ1729406).

References

[1] N. Arunkumar, K. Ramkumar, S. Hema, A. Nithya, P. Prakash, V. Kirthika: *Fuzzy Lyapunov exponent based onset detection of the epileptic seizures.* 2013 IEEE Conference on Information and Communication Technologies, ICT 2013, art. No. 6558185 (2013), 701–706.

[2] J. J. Faig, A. Moretti, L. B. Joseph, Y. Y. Zhang, M. J. Nova, K. Smith, and K. E. Uhrich: *Biodegradable Kojic Acid-Based Polymers: Controlled Delivery of Bioactives for Melanogenesis Inhibition*, Biomacromolecules *18* (2017), No. 2, 363–373.

[3] N. Arunkumar, V. Venkataraman, Thivyashree, Lavanya: *A moving window approximate entropy based neural network for detecting the onset of epileptic seizures.* International Journal of Applied Engineering Research *8* (2013), No. 15, 1841–1847.

[4] J. W. Chan, Y. Y. Zhang, and K. E. Uhrich: *Amphiphilic Macromolecule Self-Assembled Monolayers Suppress Smooth Muscle Cell Proliferation*, Bioconjugate Chemistry *26* (2015), No. 7, 1359–1369.

[5] Y. J. Zhao, L. Wang, H. J. Wang, and C. J. Liu: *Minimum Rate Sampling and Spectrum Blind Reconstruction in Random Equivalent Sampling.* Circuits Systems and Signal Processing *34* (2015), No. 8, 2667–2680.

[6] S. L. Fernandes, V. P. Gurupur, N. R. Sunder, N. Arunkumar, S. Kadry: *A novel nonintrusive decision support approach for heart rate measurement.* Pattern Recognition Letters. https: //doi.org/10.1016/j.patrec.2017.07.002 (2017).

[7] N. Arunkumar, K. Ramkumar, V. Venkatraman, E. Abdulhay, S. L. Fernandes, S., Kadry, S. Segal: *Classification of focal and non focal EEG using entropies.* Pattern Recognition Letters *94* (2017), 112–117.

[8] J. W. Chan, Y. Y. Zhang, and K. E. Uhrich: *Amphiphilic Macromolecule Self-Assembled Monolayers Suppress Smooth Muscle Cell Proliferation*, Bioconjugate Chemistry *26* (2015), No. 7, 1359–1369.

[9] M. P. Malarkodi, N. Arunkumar, V. Venkataraman: *Gabor wavelet based approach for face recognition.* International Journal of Applied Engineering Research *8* (2013), No. 15, 1831–1840.

[10] L. R. Stephygraph, N. Arunkumar: *Brain-actuated wireless mobile robot control through an adaptive human-machine interface.* Advances in Intelligent Systems and Computing *397* (2016), 537–549.

[11] W. S. Pan, S. Z. Chen, Z. Y. Feng: *Investigating the Collaborative Intention and Semantic Structure among Co-occurring Tags using Graph Theory.* International Enterprise Distributed Object Computing Conference, IEEE, Beijing (2012), 190–195.

[12] X. Du, S. Zhen, Z. Peng, C. Zhao, Y. Zhang, W. Zhe, X. Li, G. Liu, X. Li: *Acetoacetate induces hepatocytes apoptosis by the ROS-mediated MAPKs pathway in ketotic cows.* Journal of Cellular Physiology *232* (2017c), 3296–3308.

[13] Y. Y. Zhang, Q. Li, W. J. Welsh, P. V. Moghe, and K. E. Uhrich: *Micellar and Structural Stability of Nanoscale Amphiphilic Polymers: Implications for Anti-atherosclerotic Bioactivity*, Biomaterials *84* (2016), 230–240.

[14] L. R. Stephygraph, N. Arunkumar, V. Venkatraman: *Wireless mobile robot control through human machine interface using brain signals 2015 International Conference on Smart Technologies and Management for Computing, Communication*, Controls, Energy and Materials, ICSTM 2015 - Proceedings, art. No. 7225484, (2015), 596–603.

[15] X. Sun, Y. Xue, C. Liang, T. Wang, W. Zhe, G. Sun, X. Li, X. Li, G. Liu: *Histamine Induces Bovine Rumen Epithelial Cell Inflammatory Response via NF-κB Pathway.* Cellular Physiology & Biochemistry *42* (2017), No. 3, 1109–1119.

Received May 7, 2017